Real-Time Spatiotemporal Assistance for Micromanipulation Using Imitation Learning

Ryoya Mori , Tadayoshi Aoyama , *Member, IEEE*, Taisuke Kobayashi , *Member, IEEE*, Kazuya Sakamoto , Masaru Takeuchi , *Member, IEEE*, and Yasuhisa Hasegawa , *Member, IEEE*

Abstract—There has been an increasing demand for microscopic work using optical microscopes and micromanipulators for applications in various fields. However, microinjection requires skilled operators, and the considerable shortage of experts has become a recent challenge. We overcome this challenge by proposing an assistance system based on force and visual presentation using artificial intelligence technology to simplify cell rotation manipulation, which is difficult in microinjection. The proposed system employs imitation learning for an expert with a Gaussian mixture model (GMM) to obtain the ideal pipette trajectory and long short-term memory (LSTM) to infer the pipette operation at the next time step. The assistance position is calculated from the spatial component with GMM and the time-series component with LSTM. We conducted a participant experiment using mature porcine oocytes as targets for manipulation to evaluate the effectiveness of the proposed system. The results indicated that, compared to the conventional system, the proposed system reduced the pipette operation time for single-oocyte rotation and the cell damage caused by the pipette-oocyte collision by approximately 27.0% and 82.0%, respectively. Therefore, the proposed system is expected to enable beginners to reproduce high-level skills and address the shortage of experts.

Index Terms—AI-based methods, biological cell manipulation, human-centered robotics, imitation learning.

I. INTRODUCTION

MICROSCOPIC studies using optical microscopes and micromanipulators have been widely conducted in various fields [1]. Microinjection, which represents microscopic

Ryoya Mori, Tadayoshi Aoyama, Kazuya Sakamoto, Masaru Takeuchi, and Yasuhisa Hasegawa are with the Department of Micro-Nano Mechanical Science and Engineering, Nagoya University, Nagoya 464-8603, Japan (e-mail: mori@robo.mein.nagoya-u.ac.jp; tadayoshi.aoyama@mae.nagoya-u.ac.jp; sakamoto@robo.mein.nagoya-u.ac.jp; masaru.takeuchi@mae.nagoya-u.ac.jp; hasegawa@mein.nagoya-u.ac.jp).

Taisuke Kobayashi is with the Principles of Informatics Research Division, National Institute of Informatics, Tokyo 101-8430, Japan, and also with the School of Multidisciplinary Sciences, Department of Informatics, The Graduate University for Advanced Studies (SOKENDAI), Kanagawa 240-0193, Japan (e-mail: kobayashi@nii.ac.jp).
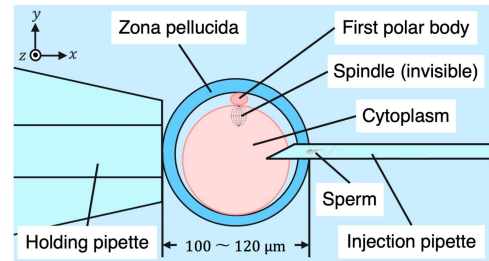
Fig. 1. Scene of ICSI: After rotating the oocyte so that the first polar body is at the 6 or 12 o'clock position to avoid damaging the spindle, the injection pipette is punctured from the 3 o'clock position to inject the sperm.

work, is a technique used to deliver small molecules such as deoxyribonucleic acid, ribonucleic acid, proteins, medicines, or other substances into the cytoplasm or nucleus of target cells. Transgenics typify this technique in the molecular biology field [2]. Microinjection involves the using an optical microscope and fine glass pipettes to inject molecules with high precision.

One application of microinjection is intracytoplasmic sperm injection (ICSI), which is a laboratory technique to inject sperm into oocytes artificially. ICSI is an assisted reproductive technology (ART) that has become the preferred technique for treating male factor infertility, replacing other ARTs such as in vitro fertilization. It has become routine for many in vitro procedures in a relatively short period, and the number of ICSI cases has increased globally [3]. Even in cases of infertility in older women or in cases wherein the sperm is not in good condition, the fertilization rate is considered to be comparatively high when using ICSI [4].

The details of the oocyte and the ICSI scene are illustrated in Fig. 1. To avoid damaging the invisible cell spindle, which plays an important role in chromosome sorting after fertilization, the oocyte is rotated around the x- and z-axis until the first visible polar body is at the 6 or 12 o'clock position. Then, puncture the polar body with an injection pipette from the 3 o'clock position while holding the oocyte with a holding pipette from the 9 o'clock position.

One challenge in this process is rotating the oocyte in three dimensions by manipulating the injection pipette while viewing a microscopic image to observe the out-of-focus condition [5]. In particular, rotating the oocyte around the x-axis is difficult because the operator must manipulate the pipette at a different z-coordinate from that of the oocyte to touch near the maximum z-coordinate point of the oocyte. Further, extreme care, such as gently touching the oocyte with the belly of the pipette and not its tip for rotation, must be employed to avoid oocyte damage,
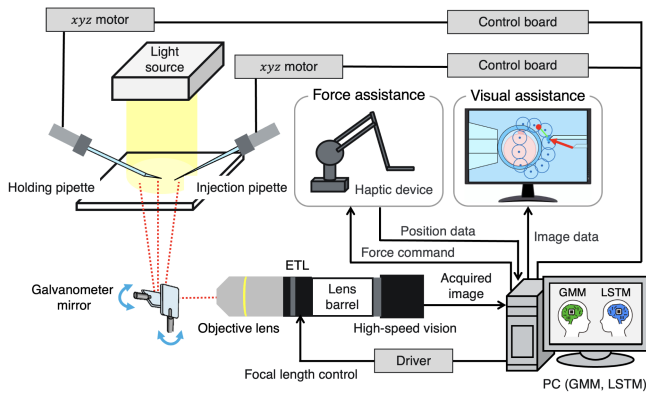
Fig. 2.   Configuration of the proposed assistance system.

Fig. 3.   Overview of the proposed assistance system.

which can affect the blastocyst development rate after fertilization [5]. Gaining the expertise to perform micromanipulation can be time-consuming for a novice. Furthermore, there is a shortage of qualified embryologists due to a limited number of experts and instructors in the field, as well as their short duration of continuous engagement. Meeting the increasing demand for ICSI has become challenging due to the shortage of qualified embryologists.

This study presents a novel spatiotemporal assistance system for oocyte rotation manipulations with force and visual presentation using imitation learning (IL) on an expert. The proposed system can assist beginners in performing similar manipulations as an expert regarding manipulation trajectories, cell rotation time, and cell damage without understanding the positional relationship between the cell and pipettes from the microscopic image. The effectiveness of the proposed system is verified through a participant experiment in terms of trajectories, rotation time, cell damage, rotation success rate, and mental workload.

II. RELATED WORKS

A. Automated Methods for Rotating Oocytes

Various nonmechanical contact-based cell-rotation methods have been studied for cell manipulation. For example, some studies employed dielectrophoresis and dielectric rotation in nonuniform electric fields [6], [7], [8] or microfluidic chips to create circulating liquid flows and rotate cells [9], [10]. Further, optical tweezers have been employed for precise pipette manipulation for cell rotation [11]. These methods have limitations such as high running costs, limited cell sizes, and inflexible cell shapes. In addition, there is no follow-up after sperm injection, which is a significant departure from conventional methods used by experts. Therefore, the effects on fertilized oocytes or newborns remain completely unknown. Various mechanical contact-based methods have been developed to automate cell rotation. The methods utilize either the frictional force generated between a substrate and an injection pipette [12] or between a substrate and a cell [13]. These methods can cause more damage to the cells than the conventional method, which only gently touches the cell with the pipette belly. However, no follow-up observations have been performed after sperm injection when using these methods. Therefore, some questions remain regarding their applicability to ICSI, which requires extreme care in manipulation. One
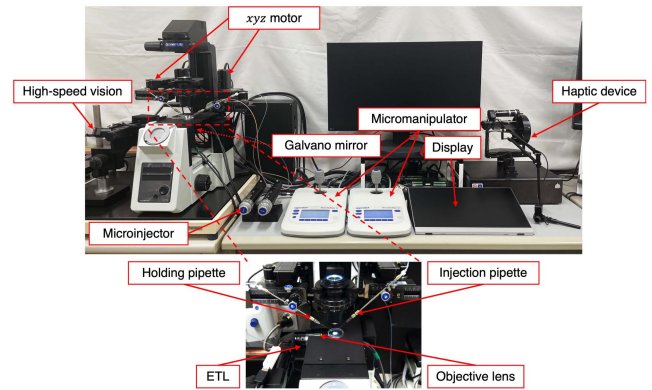
approach involves modeling the pipette and the cell to determine the optimal contact position between the pipette tip and cell, after which the pipette is manipulated automatically to rotate the cell based on detection and tracking [14]. Although designed to minimize damage to the cell, it can cause more damage than that performed by experts. Thus, this method is not suitable for ART.

B. Operation Assistance Methods for Rotating Oocytes

Automation methods mentioned above are preferred in cases where the birth of human life is not relevant, such as nuclear transplantation. However, human operators prefer ICSI. For patients with infertility, there is a significant hurdle in allowing an automation system to perform operations related to their child. In the field of ART, using another operational assistance system, instead of an automation system is considered appropriate. However, such systems have not been developed yet.

We aim to simplify the cell-rotation operation by assisting the operator based on expert IL. This approach rotates all cells (100% rotation success rate per cell) with human cooperation. It avoids damage and cost problems as the assistance systems do not require significant changes to the conventional system and the operating environment.

III. PROPOSED ASSISTANCE SYSTEM

Fig. 2 presents the configuration of our proposed operation assistance system and Fig. 3 shows the overview. The proposed system is based on the systems we developed for visual assistance [15], [16]; the proposed system comprises a haptic device connected to an injection pipette for intuitive operation (Phantom Premium 1.5 High Force, 3D Systems). This system enables the operator to manipulate the pipette through the haptic device.

As shown in Fig. 3, the conventional device for ICSI manipulation is a joystick, which enables two-dimensional operation (vertical and horizontal) and a one-dimensional operation (by rotating the upper part of the stick axis). However, the conventional device is not intuitive. Therefore, our system replaces the conventional device with a haptic device that can manipulate the three-dimensional space intuitively and provide force, thus simplifying the operation of the injection pipette.

The proposed system acquires the position coordinates of the cell and injection pipette from the camera image and motor, respectively. Subsequently, it calculates the appropriate assistance
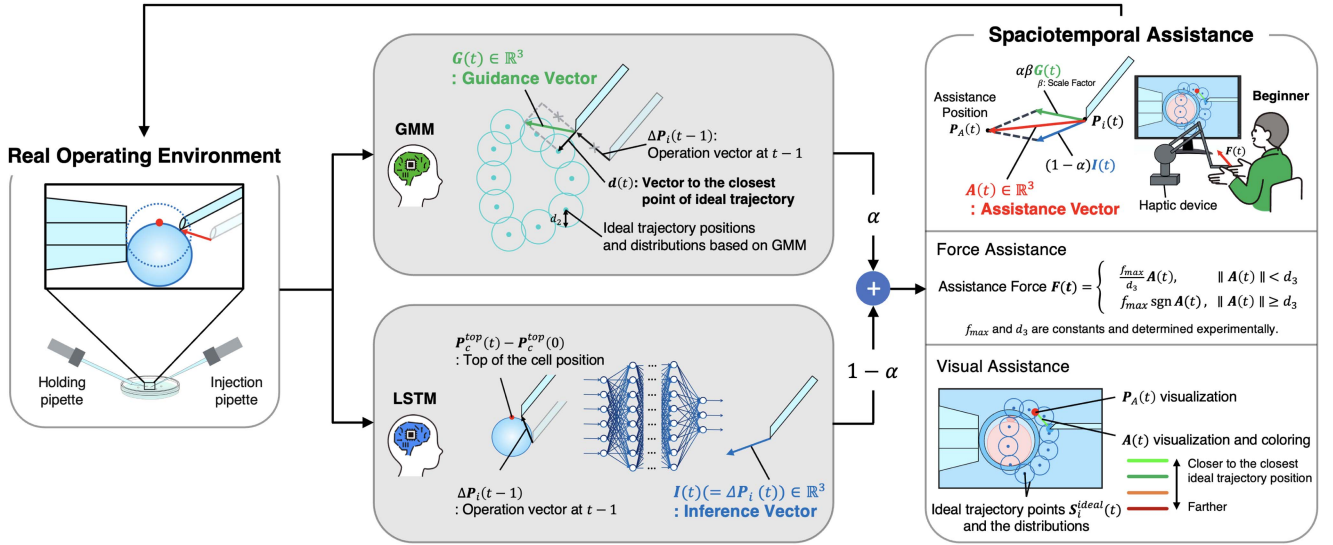
Fig. 4. Concept of the proposed spatiotemporal force and visual assistance system for micromanipuation using GMM and LSTM.

position based on artificial intelligence (AI) models, applies an appropriate force via a haptic device, and provides visual assistance on the image that the operators manipulate seeing on display. The operator manipulates the haptic device based on the provided assistance, and this manipulation of the haptic device is reflected in the actual injection pipette manipulation.

For assistance in manipulations by interacting with the operator, we propose a new system that provides spatiotemporal assistance to an operator for cell rotation around x-axis manipulation via the IL of an expert using two AI models: a Gaussian mixture model (GMM) and a long short-term memory (LSTM). Fig. 4 shows the concept of our proposed IL-based assistance system for micromanipulation. The GMM provides the spatial component of assistance and the LSTM provides the time-series component; a combination of the two provides spatiotemporal assistance. Elements such as a safety net that suppresses operations outside the ideal trajectory distribution can be included by defining the ideal trajectory using the GMM. Further, unlike end-to-end models, such as those learned only with an LSTM model with input and output position coordinates, the spatial and time-series components are assigned to the GMM and LSTM, respectively. This setup enables using the LSTM input and output as the operation quantity, allowing us to construct an LSTM model without any unlearned (out-of-distribution, OOD) regions in the position. The assistance can be stopped when the operation is interrupted because the output is close to zero, which means no manipulation is possible when the input pipette operation quantity is zero.

IV. METHODOLOGY

A. Data Collection for Expert Cell Rotation Manipulation

We collected data on the manipulation for porcine oocyte rotation about x-axis by an experienced operator. Fig. 5 shows the model of the cell and pipettes. The specific data collected include the time series of the cell top coordinates at time t: $\boldsymbol{P}_c^{top}(t)$, where the cell's z-coordinate in the camera coordinate system is at a maximum, assuming that the cell was a sphere, and the coordinates of the injection pipette tip at time t: $\boldsymbol{P}_i(t)$. When training each AI model, we use the relative coordinates from the cell top coordinates of the maximum z coordinates of the cell at time $t = 0$ at each time t: $\boldsymbol{P}_c^{top}(t) - \boldsymbol{P}_c^{top}(0)$, and the relative injection pipette's position at time t: $\boldsymbol{P}_i(t) - \boldsymbol{P}_c^{top}(0)$ to avoid depending on the absolute position of the oocyte in the captured image and the oocyte radius. Each value is obtained every 40 ms. For GMM, training was performed on data with a data length of 2000 (80.0 sec) based on the Expectation-Maximization algorithm. For LSTM, the training was performed on the data with a length of 1470 (58.8 sec), and the validation was performed on separate data with a length of 630 (25.2 sec).

B. Definition of Ideal Trajectory Positions by GMM

GMM is used to obtain the expert's ideal trajectory by approximating the probability density function of the input data with a sum of 10 Gaussian distributions. The number of Gaussian distributions was determined experimentally to distribute their means over the input data evenly. We construct the GMM model using the scikit-learn framework. The input data includes the coordinate time-series data of the injection pipette: $\boldsymbol{P}_i(t) - \boldsymbol{P}_c^{top}(0)$. The ideal trajectory corresponding to an arbitrary cell position and various radii of the cells can be obtained using the relative coordinates as input data to be trained by GMM. The maximum points (mean coordinates of each Gaussian distribution) in the learned probability density function were identified as points through which the pipette operated by the expert frequently passed. Therefore, these points can be defined as the three-dimensional ideal trajectory for the x-axis cell rotation operation, including the slight cell movement because of the contact between the cell and pipette, and the vicinity of these points within a certain distance (d_2) are defined as ideal trajectory point distributions. Fig. 6 shows the input data to train the GMM and the mean positions of each Gaussian distribution, with each axis of the graph being the respective standardized value of the pipette position coordinate $\boldsymbol{P}_i(t) - \boldsymbol{P}_c^{top}(0)$. The points distributed along the input data are successfully obtained, indicating they are appropriate for the ideal trajectory. During assistance, the set of ideal trajectory points of the injection pipette at time t: $\boldsymbol{S}_i^{ideal}(t)$ is calculated
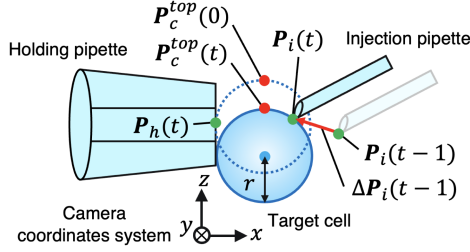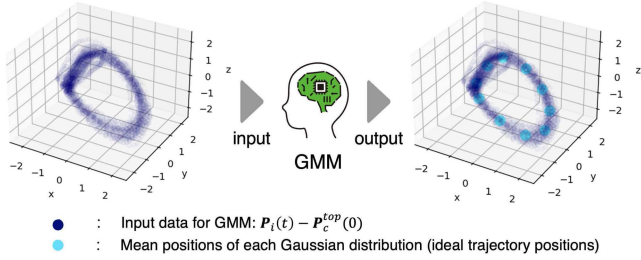
Fig. 5. Model of the cell and pipettes.

: Input data for GMM: $\boldsymbol{P}_i(t) - \boldsymbol{P}_c^{top}(0)$
: Mean positions of each Gaussian distribution (ideal trajectory positions)

Fig. 6. Input data for GMM and the mean positions of each Gaussian distribution.

Fig. 7. Time flow of expert manipulations in x-axis cell rotation, which is used for the training data of LSTM.

Fig. 8. Pipette manipulation according to the real-time inference by LSTM.

by (1), where $\boldsymbol{P}_k^{mean}$ is the coordinates of the mean positions of each Gaussian distribution ($k = 1, 2, \ldots, 10$), $\boldsymbol{P}_c^{top}(0)$ is the coordinates of top of the cell at the start of assistance, and $\Delta \boldsymbol{P}_h(t)(= \boldsymbol{P}_h(t) - \boldsymbol{P}_h(0))$ is the displacement of the holding pipette from the initial position of the assistance.

$$\boldsymbol{S}_i^{ideal}(t) = \{\boldsymbol{P}_k^{mean} + \boldsymbol{P}_c^{top}(0) + \Delta \boldsymbol{P}_h(t) \mid k = 1, 2, \ldots, 10\}. \tag{1}$$

C. Inference of an Expert's Manipulations by LSTM

LSTM, which is a recurrent neural network, was used to learn and imitate the pipette manipulations of an expert in a time series using the PyTorch framework, which includes the positional coordinate data of the cell and injection pipette when the expert performed the x-axis rotation manipulations. The LSTM model uses a six-dimensional input consisting of three-dimensional cell position $\boldsymbol{P}_c^{top}(t) - \boldsymbol{P}_c^{top}(0)$ and the three-dimensional pipette operating quantities $\Delta \boldsymbol{P}_i(t-1)(= \boldsymbol{P}_i(t) - \boldsymbol{P}_i(t-1))$, as illustrated in Fig. 5. The output dimensions of the model are set to three: $\Delta \boldsymbol{P}_i(t)$. The information related to the injection pipette in the LSTM input/output is not position coordinates but operational quantities, which allows inference without depending on the absolute position coordinates of the pipette and cell and the interruption of manipulations with assistance. Therefore, the inference by LSTM is robust against the absolute position coordinates of the pipettes, cell, and radius in the camera-acquired image.

During LSTM training, the mean absolute error was used as the loss function, and the hyperparameters were determined by Bayesian optimization using the Optuna framework with the number of layers being 2 and the number of hidden units being 32. Fig. 7 shows a real-world demonstration of operating the injection pipette according to the inference obtained using the LSTM model. Fig. 8 shows a demonstration of pipette manipulation after placing the pipette at the appropriate three-dimensional
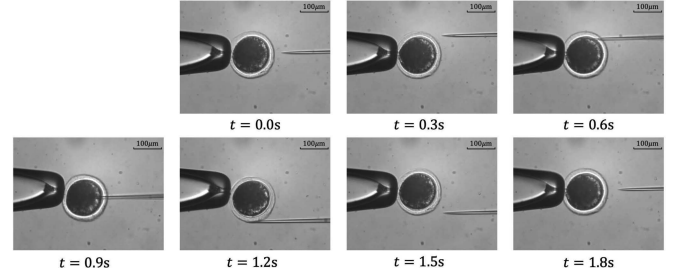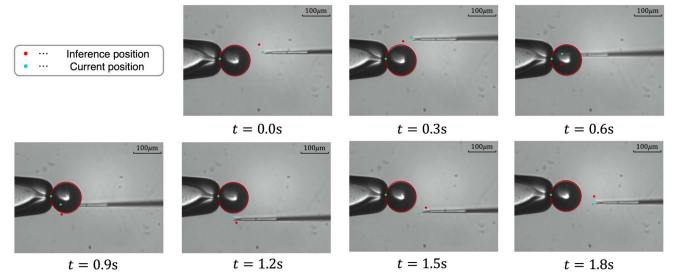
absolute coordinates for rotating the cell. The pipette is then manipulated to follow the inferred position by the LSTM. A comparison of the trajectories shown in Figs. 7 and 8 indicate that the trained LSTM model sufficiently imitated the pipette operation of the expert.

D. Assistance Position Calculation

This section presents a method to achieve spatiotemporal operation assistance by seamlessly combining guidance with the ideal trajectory defined by GMM and operation inference by LSTM. Fig. 4 shows the detail of the assistance position $\boldsymbol{P}_A(t)$ calculation. The vector (guidance vector $\boldsymbol{G}(t)$) is used for the spatial component and calculated by (2), where $\boldsymbol{d}(t)$ is the vector from the injection pipette tip to the closest ideal trajectory position and $\Delta \boldsymbol{P}_i(t-1)$ is the previous pipette operation vector. $\boldsymbol{d}(t)$ guides the injection pipette towards the ideal trajectory, whereas $\Delta \boldsymbol{P}_i(t-1)$ ensures smooth guidance during operation.

$$\boldsymbol{G}(t) = \boldsymbol{d}(t) + \Delta \boldsymbol{P}_i(t-1). \tag{2}$$

The three-dimensional operation quantity obtained by LSTM (inference vector $\boldsymbol{I}(t)$) is directly used for the time-series component.

As indicated in (3), the assistance vector $\boldsymbol{A}(t)$ is calculated by synthesizing the guidance vector $\boldsymbol{G}(t)$ and the inference vector $\boldsymbol{I}(t)$ multiplied by the weight coefficients α and $1 - \alpha$, respectively, where β represents a scale factor. The weight coefficient α varies according to the Euclidean distance $\|\boldsymbol{d}(t)\|$ (μm) between the pipette and nearest ideal trajectory point, as shown in (4), where d_1 and $d_2(< d_1)$ are constants. The assistance position $\boldsymbol{P}_A(t)$ is calculated using (5).

$$\boldsymbol{A}(t) = \alpha \beta \boldsymbol{G}(t) + (1 - \alpha)\boldsymbol{I}(t). \tag{3}$$
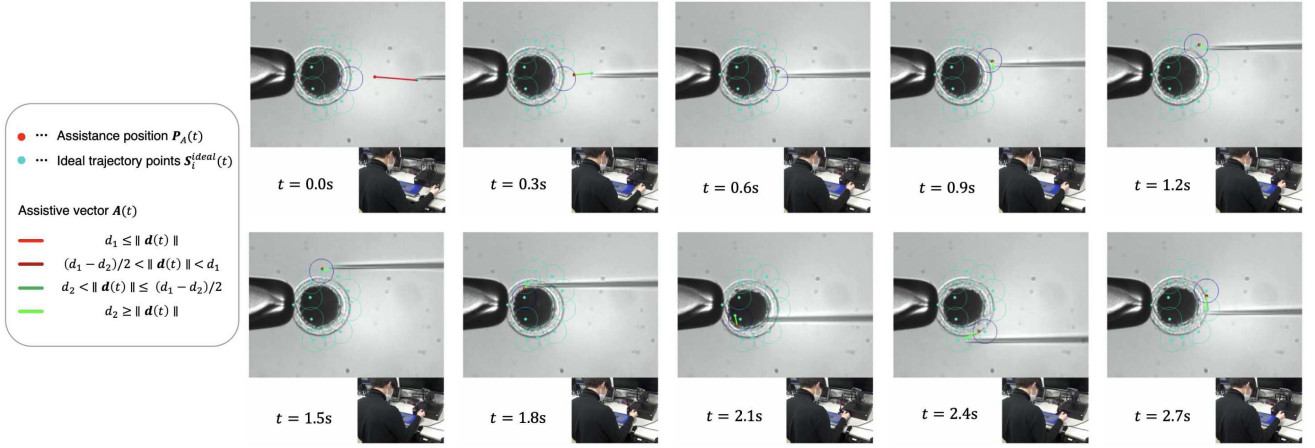
Fig. 9. Time flow of cell rotation with the proposed force and visual spatiotemporal assistance system.

$$\alpha = \begin{cases} 1.0 & \text{if } d_1 \leq \|\boldsymbol{d}(\text{t})\| \\ \dfrac{0.8\|\boldsymbol{d}(t)\|}{d_1 - d_2} + \dfrac{0.2d_1 - d_2}{d_1 - d_2} & \text{if } d_2 < \|\boldsymbol{d}(\text{t})\| < d_1 \\ 0.2 & \text{if } d_2 \geq \|\boldsymbol{d}(\text{t})\|. \end{cases} \tag{4}$$

$$\boldsymbol{P}_A(t) = \boldsymbol{P}_i(t) + \boldsymbol{A}(t). \tag{5}$$

When the pipette is outside the ideal trajectory distribution and far away ($d_1 \leq \|\boldsymbol{d}(t)\|$), $\boldsymbol{A}(t)$ is calculated, setting α to 1.0 to guide the pipette to the ideal trajectory distribution. In closer regions ($d_2 < \|\boldsymbol{d}(t)\| < d_1$), the pipette is guided smoothly into the ideal trajectory distribution by varying α linearly with $\|\boldsymbol{d}(t)\|$. Then, within the ideal trajectory distribution ($d_2 \geq \|\boldsymbol{d}(t)\|$), α is kept constant (0.2) for eliminating the unnecessary changes in α during transitions of the closest ideal trajectory point from the pipette, and for preventing the chattering of $\boldsymbol{P}_A(t)$. Further, setting α to 0.2 instead of 0.0 within the ideal trajectory distribution retains the guiding component from the edge of the ideal trajectory distribution to the ideal trajectory point for ensuring spatial assistance.

Note that the OOD inputs to the LSTM may include abrupt or irrelevant manipulations. However, if the LSTM is guided by such manipulations or the unstable output they produce, the pipette may deviate from the ideal trajectory distribution and switch to GMM assistance, thereby ensuring safety.

E. Force and Visual Presentation Assistance

1) Force Presentation: The proposed system provides operational assistance through force and visual presentation based on $\boldsymbol{A}(t)$. For force presentation, the magnitude and direction of the assistance force $\boldsymbol{F}(t)$ are determined by $\|\boldsymbol{A}(t)\|$ (μm), as shown in (6), where $f_{\max}$ represents the maximum force magnitude and d_3 (μm) is a constant.

$$\boldsymbol{F}(t) = \begin{cases} \dfrac{f_{\max}}{d_3}\boldsymbol{A}(t) & \text{if } \|\boldsymbol{A}(\text{t})\| < d_3 \\ f_{\max}\text{sgn}\boldsymbol{A}(t) & \text{if } \|\boldsymbol{A}(\text{t})\| \geq d_3. \end{cases} \tag{6}$$

Simple force assistance with a constant force is employed to avoid operator discomfort caused by frequent changes in the assistance force size. When $\|\boldsymbol{A}(t)\|$ is small (less than d_3), force

proportional to $\|\boldsymbol{A}(t)\|$ is applied to the vector $\boldsymbol{A}(t)$ to prevent chattering of the force presentation when the assistance position moves slightly near the pipette.

2) Visual Presentation: The visual presentation includes displaying $\boldsymbol{A}(t)$ and $\boldsymbol{P}_A(t)$, and coloring it based on the Euclidean distance $\|\boldsymbol{d}(t)\|$ to the nearest ideal trajectory point from the pipette tip. $\boldsymbol{A}(t)$ is red when $d_1 \leq \|\boldsymbol{d}(t)\|$, orange when $(d_1 - d_2)/2 < \|\boldsymbol{d}(t)\| < d_1$, sage green when $d_2 < \|\boldsymbol{d}(t)\| \leq (d_1 - d_2)/2$, and green when $\|\boldsymbol{d}(t)\| \leq d_2$, allowing the operator to easily see and understand intuitively how far the pipette is from the closest ideal trajectory point. The force $\boldsymbol{F}(t)$ is not calculated directly using GMM and LSTM to visually assist with $\boldsymbol{A}(t)$ and $\boldsymbol{P}_A(t)$.

The ideal trajectory points and their distributions are also displayed, and the nearest ideal trajectory points and their distributions are colored to provide additional information about where the pipette is guided by $\boldsymbol{d}(t)$. Based on the ideal trajectory points and their distributions, $\boldsymbol{A}(t)$ and $\boldsymbol{P}_A(t)$, and their coloring, the operator can obtain a comprehensive image of the assistance, which cannot be fully recognized only using force presentation. This results in the operator reducing their anxiety when receiving assistance and increasing the likelihood of following the assistance position even if they are unfamiliar with the haptic device. Fig. 9 shows the scene of beginner's operation with the proposed assistance system.

V. EVALUATION

A. Experiment

We conducted a participant experiment using mature porcine oocytes, whose size is generally 134.59 ± 11.87 μm [17], as the target for manipulations to evaluate the effectiveness of the proposed micromanipulation spatiotemporal assistance system. The experiment was conducted under the following three conditions.

(a) Using the existing manipulation system with a joystick
(b) Using the force and visual assistance system with a haptic device with only LSTM
(c) Using the force and visual assistance system with a haptic device with GMM and LSTM
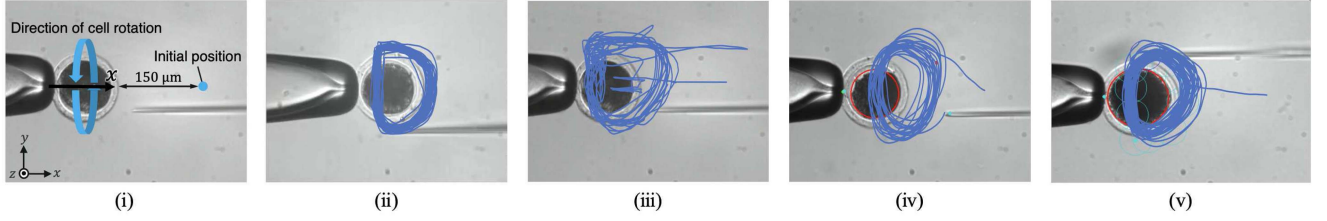
Fig. 10. (i): Cell rotation direction and the injection pipette initial position in the experiment, (ii): Pipette trajectory of an expert in condition (a), (iii): Pipette trajectory of a beginner in condition (a), (iv): Pipette trajectory of a beginner in condition (b), and (v): Pipette trajectory of a beginner in condition (c).

Assistance using ideal trajectory points obtained from the GMM ignores the time series and shows a wobbly trajectory because of the lack of attractor-like guidance. The use of GMM alone cannot imitate the pipette manipulation of an expert, and it is impossible to make stable and smooth manipulation. Therefore, the GMM-only assistance system was excluded from the experimental conditions in this study. Condition (b) shows an assistance system that provides force and visual assistance based on the inferred position of the LSTM model, which infers the absolute position $P_i(t+1) - P_c^{top}(0)$ of the pipette at the next time step by inputting the current $P_c^{top}(t) - P_c^{top}(0)$ and $P_i(t) - P_c^{top}(0)$. When the operational quantities are input/output of the LSTM, it is crucial for the operator to first have a clear understanding of the 3D positional relationship between the pipette and the oocyte. The pipette must be positioned properly by the operator, as in condition (a), because the LSTM infers the next operational quantities independently of the current pipette position. Therefore, condition (b) cannot guide the pipette to the proper absolute position if the operational quantities are input/output of the LSTM. This system was designed to verify the validity of the combination of the ideal trajectory using GMM and the input/output of the LSTM model in (c). Condition (b) includes the characteristics of most of the position-dependent trajectory imitation methods proposed so far [18], [19]. The LSTM model in (b) was trained using the training data with the pipette position coordinates, which were the same manipulations as in (c); the hyperparameters were obtained by Bayesian optimization, similar to that in (c). For (c), $d_1 = 60\,\mu m$, $d_2 = 30\,\mu m$, $\beta = 0.5$, $f_{max} = 0.8$ N, and $d_3 = 10\,\mu m$ are determined experimentally.

The task was to rotate the cell about the x-axis by manipulating the injection pipette, as shown in Fig. 10(i), using the respective device in each condition. The initial position of the injection pipette was determined randomly from five initial coordinates that the x- and y-coordinates are the same position as the center of the cell, as shown in Fig. 10(i), and differ only in z-coordinates such that the initial position is not covered and known to the novice operator. The five initial coordinates are set as follows:

① From the z-coordinate of the cell
② From 150 μm added to the z-coordinate of the cell
③ From 150 μm minus from the z-coordinate of the cell
④ From 300 μm added to the z-coordinate of the cell
⑤ From 300 μm minus from the z-coordinate of the cell

Six participants with no prior experience in micromanipulation (aged 20–25 years) performed the task five times for each condition. The order of conditions for each participant was non-overlapping to reduce order bias.

The evaluation criteria consisted of task completion time, pipette-cell collision rate P_c, the success rate of the cell rotation operation P_s, as calculated in (7) respectively, and mental workload assessed using the weighted workload (WWL) in NASA Task Load Index (NASA-TLX). Success is defined as a case where the pipette contacts the cell at the belly of the pipette, and the cell rotates only around the x-axis. A collision is defined as a case that does not apply to success, and there is contact between the cell and the pipette. Since the required rotation angle differs from time to time, a large rotation is not always better, nor is a smaller rotation better. For the sake of a consistent benchmark, the evaluation was purely based on whether the rotation operation was successful or not.

$$P_c = \frac{N_c}{N_t}, P_s = \frac{N_s}{N_t}. \qquad (7)$$

N_c: The number of pipette-cell collisions without cell rotation about x-axis in a task
N_t: The number of attempts for rotating the cell in a task
N_s: The number of successful cell rotations about the x-axis in a task

In microinjection, the operator must inject many cells in a day, and when the cells are not in the body, it damages them. Thus, the manipulation time is very significant. Further, cell damage is crucial for blastocyst development. A short task completion time and a low pipette-cell collision rate are essential to develop assistance systems for ICSI.

B. Results and Discussions

The proposed system improved the consistency of the pipette operation trajectories, as shown in Fig. 10. Fig. 10(ii) shows the pipette trajectory of an expert in x-axis cell rotation manipulations, whereas Figs. 10(iii), 10(iv), and 10(v) show the pipette trajectories of a beginner under condition (a), (b), and (c), respectively. The figures suggest that (c) reduces the trajectory variability of beginners compared to other systems and unnecessary collision to the cell. This improvement allows beginners to perform manipulations that closely resemble those of an expert in terms of trajectory stability, geometry, and safety.

Figs. 11(i), 11(ii), 11(iii), and 11(iv) and Tables I, II, III, and IV present the results of the experiment. The box plots of task completion time, rotational success rate, pipette-cell collision rate, and mental workload for each condition are shown in the figures. We utilized the Steel-Dwass test for statistical evaluation, a multiple comparison test.

1) Task Completion Time: The test results indicate that (c) significantly reduced the task completion time compared to both condition (a) and (b), as shown in Fig. 11(i). This reduction in the completion time can be attributed to the proposed system
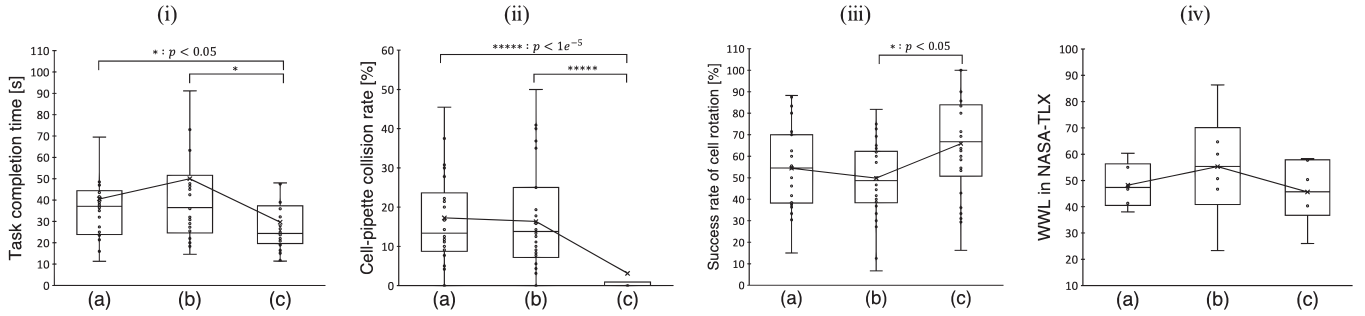
Fig. 11.   (i): Box plot of task completion time, (ii): Box plot of pipette-cell collision rate, (iii): Box plot of the success rate of cell rotation, (iv): Box plot of WWL in NASA-TLX.

TABLE I
TASK COMPLETION TIME

	Condition (a)	Condition (b)	Condition (c)
Participant A	71.5 s	82.8 s	42.4 s
Participant B	41.5 s	45.3 s	29.2 s
Participant C	33.4 s	37.1 s	19.2 s
Participant D	35.0 s	38.7 s	36.0 s
Participant E	27.0 s	47.7 s	24.4 s
Participant F	34.6 s	48.6 s	26.5 s
Average	40.5 s	50.0 s	29.6 s

TABLE III
SUCCESS RATE OF CELL ROTATION

	Condition (a)	Condition (b)	Condition (c)
Participant A	42.6 %	40.0 %	52.3 %
Participant B	52.7 %	63.7 %	70.2 %
Participant C	55.1 %	51.8 %	69.5 %
Participant D	50.5 %	43.9 %	67.6 %
Participant E	64.9 %	46.6 %	58.7 %
Participant F	60.4 %	53.1 %	77.0 %
Average	54.4 %	49.8 %	65.9 %

TABLE II
PIPETTE-CELL COLLISION RATE

	Condition (a)	Condition (b)	Condition (c)
Participant A	29.8 %	10.3 %	2.28 %
Participant B	15.7 %	9.91 %	3.33 %
Participant C	15.3 %	17.5 %	5.82 %
Participant D	20.4 %	20.0 %	0 %
Participant E	11.1 %	11.3 %	7.33 %
Participant F	11.3 %	29.0 %	0 %
Average	17.3 %	16.3 %	3.13 %

TABLE IV
WWL IN NASA-TLX

	Condition (a)	Condition (b)	Condition (c)
Participant A	55.0	86.3	50.3
Participant B	60.0	40.3	60.3
Participant C	23.3	41.3	26.0
Participant D	57.7	46.7	50.7
Participant E	48.0	58.3	46.7
Participant F	41.0	64.7	38.0
Average	47.5	56.3	45.3

being able to guide the pipette immediately from the arbitrary initial position to the appropriate three-dimensional positions for the x-axis rotation operation.

For condition (a), it is necessary to understand the three-dimensional positional relationship between the injection pipette and the cell by observing the relationship between the out-of-focus areas in the microscopic image. It requires time to determine whether the pipette is above or below the cell. For condition (b), unlearned (OOD) inputs in the camera coordinate system in the acquired image can be input to the LSTM because the inputs for LSTM are position coordinates, particularly in the initial positions ④ and ⑤; this makes the inference unstable. The system may take time to draw inferences near the cell, the learned (in-distribution, ID) area.

2) Cell-Pipette Collision Rate: The cell-pipette collision rate is significantly reduced in condition (c) compared to both (a) and (b), as shown in Fig. 11(ii). Operating under condition (a) is very difficult for beginners because they must understand the three-dimensional positional relationship from a microscopic image. This complexity is believed to increase the frequency of pipette collisions with the cells caused by mispositioning. For condition (b), OOD inputs were given to the LSTM model and the inference was unstable, causing the pipette to collide with

the cell. Therefore, P_c in condition (c) significantly reduced the probability of the pipette colliding with the cell relative to (b).

3) Cell Rotation Manipulation Success Rate: The test results indicate that condition (c) helped significantly increase the cell rotation success rate P_s compared to (b), as shown in Fig. 11(iii). The success rate in (c) did not increase significantly compared to that in (a) because the AI models did not fit all participants well. Only participant E did not increase the success rate P_s under (c) compared with that in (a). Moreover, participant E showed a smaller decrease than the others in task completion time and pipette-cell collision rate. This finding suggests that the AI models may not fit this person well because the training data for AI models were created by only one expert. Thus, future work must increase the number of experts for IL and develop an assistance system that considers individual differences in operations.

4) Mental Workload: The mental workload under (c) was not significantly reduced compared to the other conditions, as shown in Fig. 11(iv). However, there was an overall trend toward a decrease in mental workload, especially for (c) compared to (b). In addition, the mean, maximum, and minimum workloads decreased for (c) compared to (a). This slight decrease in the mean and the smaller maximum and minimum values for those in (c) suggest that the mental and intellectual workload may be

the same or less than those in (a). Thus, one can operate in (c) with the same mental workload as that in (a).

5) Overview: The evaluation experiment showed that the proposed system led to an ideal trajectory from an arbitrary pipette position, simplifying and improving the efficiency of the operation. Further, the system showed high stability concerning the pipette position compared to the LSTM-based assistance system. The spatial guidance to the ideal trajectory by GMM and stability of LSTM inference can help reduce cell damage, contributing greatly to blastocyst development rates attributed to a lower cell collision rate. These results confirm that, compared to LSTM, which infers absolute position coordinates, as in (b), by using operation quantities as LSTM inputs and outputs, OOD inputs are not inputs unless an abrupt or irrelevant operation is performed. Further, high robustness can be added to the absolute pipette coordinates by obtaining an ideal trajectory with the GMM and performing guidance. Although the mental workload was not reduced significantly under the other conditions, it was confirmed that the proposed system could operate with the same mental workload as the conventional system. These results confirm that the proposed system effectively simplifies cell-rotation operations, increases efficiency, and reduces cell damage at the same mental workload as the conventional system.

VI. CONCLUSION

We developed a novel spatiotemporal assistance system for pipette operation to rotate oocytes around the x-axis by combining GMM and LSTM. Our system guides the pipette from an arbitrary position to an ideal trajectory distribution defined by the GMM. Then, it assists the manipulation by LSTM inference while incorporating guidance to the ideal trajectory. This approach ensures that the assistance is robust to changes in the pipette position. The evaluation results indicated that the proposed system achieved a reduction of approximately 27.0% in the time to rotate the oocyte once and a reduction of approximately 82.0% in the number of triggers that may cause cell damage caused by pipette-cell collisions compared to other systems. Thus, our proposed system simplifies and improves the efficiency of cell rotation while reducing cell damage compared to the conventional and LSTM-based assistance systems. The pipette trajectory during the experiment showed that even a beginner could operate the pipette with a trajectory more similar to that of experts than with the conventional system. This system can be applied to other micromanipulations which need cell rotation. Our future work is to realize assistance for individual differences in operations and apply this system to other micromanipulations.

REFERENCES

[1] W. M. E. Shakweer, A. Y. Krivoruchko, S. M. Dessouki, and A. A. Khattab, "A review of transgenic animal techniques and their applications," *J. Genet. Eng. Biotechnol.*, vol. 21, no. 1, 2023, Art. no. 55.

[2] Q. Xu, *Review of Microinjection Systems*. Berlin, Germany: Springer Int. Publishing, 2018, pp. 15–47.

[3] G. D. Adamson et al., "International committee for monitoring assisted reproductive technology: World report on assisted reproductive technology," *Fertility Sterility*, vol. 110, pp. 1067–1080, 2018 .

[4] A. C. Van Steirteghem et al., "High fertilization and implantation rates after intracytoplasmic sperm injection," *Hum. Reproduction*, vol. 8, no. 7, pp. 1061–1066, 1993.

[5] D. P. Braga et al., "Use of pig oocytes for training new professionals in human assisted reproduction laboratories," *Fertility Sterility*, vol. 88, no. 5, pp. 1408–1412, 2007.

[6] L. Huang, P. Zhao, and W. Wang, "3D cell electrorotation and imaging for measuring multiple cellular biophysical properties," *Lab Chip*, vol. 18, no. 16, pp. 2359–2368, 2018.

[7] K. Huang, I. A. Ajamieh, Z. Cui, J. Lai, J. K. Mills, and H. K. Chu, "Automated embryo manipulation and rotation via robotic nDEP-tweezers," *IEEE Trans. Biomed. Eng.*, vol. 68, no. 7, pp. 2152–2163, Jul. 2021.

[8] Y. T. Chow et al., "Liquid metal-based multifunctional micropipette for 4D single cell manipulation," *Adv. Sci.*, vol. 5, no. 7, 2018, Art. no. 1700711.

[9] Y. Yaxiaer, Y. Kanda, and K. Morishima, "Hydrodynamic vertical rotation method for a single cell in an open space," *Microfluidics Nanofluidics*, vol. 20, 2016, Art. no. 74.

[10] T. Hayakawa, S. Sakuma, and F. Arai, "On-chip 3D rotation of oocyte based on a vibration-induced local whirling flow," *Microsystems Nanoeng.*, vol. 1, no. 1, pp. 1–9, 2015.

[11] X. Chen, G. Xiao, X. Han, W. Xiong, H. Luo, and B. Yao, "Observation of spin and orbital rotation of red blood cell in dual-beam fibre-optic trap with transverse offset," *J. Opt.*, vol. 19, no. 5, 2017, Art. no. 055612.

[12] Z. Wang, C. Feng, R. Muruganandam, W. T. Ang, S. Y. M. Tan, and W. T. Latt, "Three-dimensional cell rotation with fluidic flow-controlled cell manipulating device," *IEEE/ASME Trans. Mechatron.*, vol. 21, no. 4, pp. 1995–2003, Aug. 2016.

[13] I. Abu Ajamieh, B. Benhabib, and J. K. Mills, "Automatic system for the blastocyst embryo manipulation and rotation," *Ann. Biomed. Eng.*, vol. 48, pp. 426–436, 2020.

[14] H. Gong et al., "Automatic cell rotation based on real-time detection and tracking," *IEEE Robot. Automat. Lett.*, vol. 6, no. 4, pp. 7909–7916, Oct. 2021.

[15] T. Aoyama et al., "Micromanipulation system capable of simultaneously presenting high-resolution and large field-of-view images in real-time," *IEEE Access*, vol. 11, pp. 34274–34285, 2023.

[16] T. Fujishiro, T. Aoyama, K. Hano, M. Takasu, M. Takeuchi, and Y. Hasegawa, "Microinjection system to enable real-time 3D image presentation through focal position adjustment," *IEEE Robot. Automat. Lett.*, vol. 6, no. 2, pp. 4025–4031, Apr. 2021.

[17] R. Grabowska, B. Blaszczyk, T. Stankiewicz, T. Banas, S. Hale, and J. Udala, "Quality of oocytes in prepubertal and pubertal swine," *Turkish J. Vet. Animal Sci.*, vol. 40, no. 1, pp. 89–94, 2016.

[18] S. Calinon, F. Guenter, and A. Billard, "On learning, representing, and generalizing a task in a humanoid robot," *IEEE Trans. Syst., Man, Cybern., Part B. (Cybern.)*, vol. 37, no. 2, pp. 286–298, Apr. 2007.

[19] R. Wang, Y. Wu, W. L. Chan, and K. P. Tee, "Dynamic movement primitives plus: For enhanced reproduction quality and efficient trajectory modification using truncated kernels and local biases," in *Proc. IEEE/RSJ Int. Conf. Intell. Robots Syst.*, 2016, pp. 3765–3771.